


Research Article

Fault Size Estimation of Bearings Using Multiple Decomposition Techniques with Artificial Neural Network

Suchi Mishra ¹, Rahul Dubey,² Preety D. Swami,³ and Alok Jain¹

¹Department of Electronics and Instrumentation Engineering, SATI, Vidisha, India

²Department of Electronics Engineering, MITS, Gwalior, India

³Department of Electronics and Communication Engineering, UIT RGPV, Bhopal, India

Correspondence should be addressed to Suchi Mishra; mishrasuchi08@gmail.com

Received 14 April 2022; Revised 16 May 2022; Accepted 30 May 2022; Published 17 June 2022

Academic Editor: Punit Gupta

Copyright © 2022 Suchi Mishra et al. This is an open access article distributed under the Creative Commons Attribution License, which permits unrestricted use, distribution, and reproduction in any medium, provided the original work is properly cited.

A running machine generates multi-frequency vibration signals which can be captured by accelerometers. Empirical mode decomposition, wavelet decomposition, and wavelet packet decomposition are the commonly used methods to decompose the multi-frequency signal. Quick fault classification, accurate signal decomposition, and fault size detection are still a problem in machines with rotary components. In the proposed work, fault diameter in rotary part of machine is detected and classified using the machine learning methods. In the first stage, we have employed empirical mode decomposition (EMD) for high-frequency noise removal. Residue signal is obtained by removing first IMF from base signal considering first IMF as a high-frequency noisy signal, followed by wavelet decomposition. Entropy of the wavelet coefficient obtained from 3rd level decomposition of residue signal is calculated which acts as an input parameter to the machine learning techniques to determine the diameter for fault. Three different sets have been taken for inner race, outer race, and ball race correspondingly. The proposed method classifies and detects the fault diameter up to 99.5%. The proposed method can be used for different types of continuous as well as discrete wavelets.

1. Introduction

The main objective of maintenance department in industries is to keep machineries running. Machine failure makes unwanted downtime across the industries with high maintenance cost. Rolling bearing is considered as a vital component of rotating machines. Several kinds of faults exist in bearings. The faults in the bearing decrease the accuracy and performance of the machine.

Bearing fault detection is done using various signal processing techniques. Various available methods to analyse the bearing fault signals are categorized in time-frequency domain [1, 2], time domain [3–5], and frequency domain [6–9]. Image processing techniques have also been explored in works for diagnosis and detection of bearing fault [10, 11].

The use of vibration signal in the analysis of bearing faults is also reported in the literature. These vibration signals are recorded using accelerometer which may have noisy background. Kurtosis analysis is also one of the

methods applied for the early-stage detection of faults in bearing. In earlier research studies, it is already proved that for kurtosis value more than three, faults are present in the vibration signal [12].

Wavelet transform (WT) is applicable for investigation of non-stationary signals. Wavelet transform is used for the decomposition of signal into approximation and detailed coefficient. Application of wavelet transforms in the detection of bearing faults is also reported by Kumar Jha and Swami [13].

Various statistical parameters extracted from the wavelet coefficients of vibration signals are utilized for different wavelet functions for fault detection [14].

Parey et al applied the combination of artificial Intelligence methods with maximum energy to Shannon entropy extracted from wavelet coefficients for the ball bearing fault classification [15].

WT has been extensively used in signal denoising. In [16], Ali Alnuaim et al suggested a procedure for rolling

bearing fault diagnosis evolved from wavelet denoising. Wavelet-based function is chosen from impulse response of the bearing system. The authors optimized damping factor and central frequency of wavelet on the basis of kurtosis maximization criteria. Simulated and real rolling vibration signals were both used in [16] to judge the performance of the proposed approach.

In [17], reshaping of Morlet wavelet is done by using Shannon entropy. Li and Yin extracted a weak fault signature from rolling bearing from wavelet filter bank [17]. Singular value decomposition is utilized to obtain the periodicity of the signal in the proposed approach in [17].

Enhancement of impulsive features and suppression of residual noise were achieved by Rafiee et al. using Morlet wavelet for detection of bearing fault [18]. Jiang et al. optimized the wavelet filter by eliminating the interferential vibration using differential evolution and retrieved the characteristics of fault present in the signal.

In [19], Kankar et al. used genetic algorithm to enhance the parameters of Morlet wavelet to maximize the sparsity measurement value. The optimal wavelet filter provides the modulus of the wavelet coefficients which is used to pull out the envelope. Finally, for enhancement of the visual inspection, the ability of bearing fault characteristic frequencies of a non-linear function is utilized.

Faulty vibration signals recorded through accelerometer for rolling bearings with respect to different fault condition were preprocessed via Laplace-wavelet transform for feature extraction by Shukla and Dixit [20]. Obtained characteristics from time and frequency domains are utilized as an input to artificial neural network for fault classification. A feedforward multi-layer perceptron neural network, which consists of three layers, was used for the categorization in [20].

Lempel–Ziv complexity along with CWT was utilized to characterize the bearing faults in [21]. CWT was utilized to find best location of faults and to remove interferences of noise and irrelevant signal components. The envelope and high-frequency carrier signal are drawn from wavelet coefficient followed by Lempel–Ziv complexity value calculation for all.

The hybrid CWT-SVM method was proposed by Qiu et al. for bearing fault detection in induction motor in [22].

The CWT with autocorrelation improvement was given by He et al. in [23] to allow minor defect detection of bearings. The coefficients of CWT are calculated after reducing dimensions of vibration signal. The ratio of energy to Shannon entropy was applied as a parameter to select the base wavelet followed by extraction of the statistical feature from wavelet coefficient. In the last stage, soft computing techniques were applied to do the classification of bearing faults [24].

The detection of bearing fault using morphological wavelet slicing was proposed by Tiwari and Shukla in [25]. Li et al. proposed a multi-scale autocorrelation approach for the analysis of the bearing fault. Fourier transform of extracted temporal components is evaluated to view morphological slices in frequency domain. Its three-dimensional representation was reduced by the presence of noise. Hence, autocorrelation function was used to produce a multi-scale

autocorrelation spectrogram to maximize the autocorrelation values of all frequencies.

For non-linear and non-stationary signals, Peter and Wang [26] suggested an EMD technique that overcomes disadvantages of wavelet transform. Al Raheem et al. [27] used the footprint of Hilbert plot as a metric to characterize distinct ball bearing faults. The suggested approach is estimated to be 99.98% efficient [27].

The polar diagram in [28] is used to improve the periodic transient signals caused by bearing defects. In the method proposed in [28], signal is represented in time scale domain using CWT, and then it maps wavelet coefficient into polar diagram. Transient characteristics would thus be synchronously improved at a definite area if mapping time period equals that of transient vibrations.

Stalin et al. proposed adaptive wavelet to improve impulsive features generated due to bearing [29]. The proposed scheme enhanced the impulsive components and simultaneously depressed the noise.

Application of artificial neural network for the classification of rolling bearing faults can be extensively found in the literature [30–33]. In [30], Konar and Chattopadhyay used PCA along with SVD for bearing fault detection. Li et al. applied the EMD method followed by singular value decomposition. Elman neural network is used in later stage for classification of bearing faults. Classification of ball bearing faults is also done using various artificial neural network methods in [32, 33].

The detection of fault size is still unexplored in the literature. In the proposed work, EMD is used on bearing signal to eliminate high-frequency noisy component. First, IMF is measured to be a high-frequency signal; therefore, it is removed from the bearing signal to get the residue [34]. The three-level wavelet decomposition of the residue signal is done. The entropy of the third level wavelet coefficient has been calculated which is further utilized as an input parameter for feedforward neural network to categorize bearing signal into respective classes [35].

This paper is organized as follows. In Section 2, EMD, WT, and features based on entropy are discussed. In Section 3, the proposed method is discussed. In Section 4, results and discussion are given, followed by conclusion and future scope in Section 5.

2. Theory

2.1. Empirical Mode Decomposition. Peter and Wang presented the decomposition of a signal through the EMD method in [26]. The EMD method decomposed a signal into an IMF from high-frequency component to low-frequency component. There are two necessary conditions for the component to be IMF, written below:

- (i) Number of zero crossing and number of extrema in the each signal in the whole dataset essentially either equal or differ at most by one.
- (ii) At any point, the mean value of envelope explained by local maxima and local minima is zero.

The EMD algorithm is summarized below.

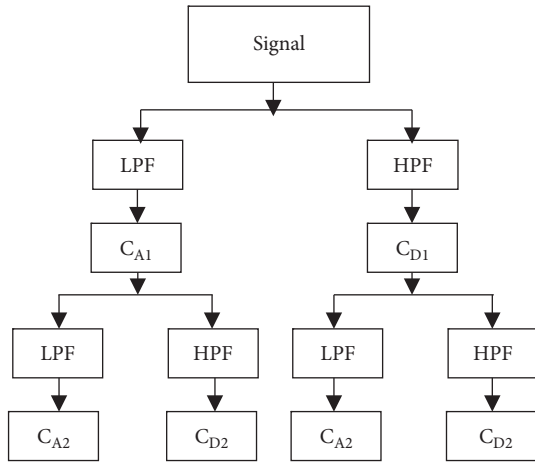


FIGURE 1: Two-dimensional wavelet decomposition.

Signal $x(t)$ is subjected to calculate every probable extrema. Lower and upper envelopes $X_{\min}(t)$ and $X_{\max}(t)$, respectively, are obtained through interpolation among minima and corresponding maxima [36]. The mean value $a(t)$ of the envelope is determined using equation (1), which is further deducted from signal $x(t)$ to get $h(t)$ using equation (2).

$$a(t) = \frac{X_{\min}(t) + X_{\max}(t)}{2}, \quad (1)$$

$$h(t) = x(t) - a(t). \quad (2)$$

It is checked whether $h(t)$ is an IMF. If it is an IMF, the residual signal $r(t)$ is drawn by repeating the above steps using equation (3), or else replace $x(t)$ with $h(t)$, and do entire process again.

$$r(t) = x(t) - h(t). \quad (3)$$

$IMF_1(t), IMF_2(t), IMF_3(t), \dots, IMF_N(t)$ are different frequency components of $x(t)$ from high-frequency component to low-frequency component. Residual component of a signal x is used to display its central tendency (t). By combining all IMFs and residual r , the original signal $x(t)$ may be reconstructed (t).

2.2. Wavelet Transform (WT). The wavelet is a progressive research filed for the researcher in the engineering over last 20 years. Some of the researchers have contributed substantially to the use of the wavelet transform in bearing fault identification [37]. Wavelet transform is a mathematical tool that changes signals from time domain to time-frequency domain. Wavelet transform is broadly classified as CWT, DWT, and WPT [38]. Wavelet transform passes one-dimensional signal via filter bank consisting of LPF and HPF. The signal component passing through the low-pass filter is recognized as approximation coefficient (C_{A1}) while the component extracted from the high-pass filter is recognized as detailed coefficient (C_{D1}). This is one-level wavelet decomposition, and achieved coefficients are known as first-level wavelet coefficients [39]. Further, the approximation and detailed coefficient is passed again through

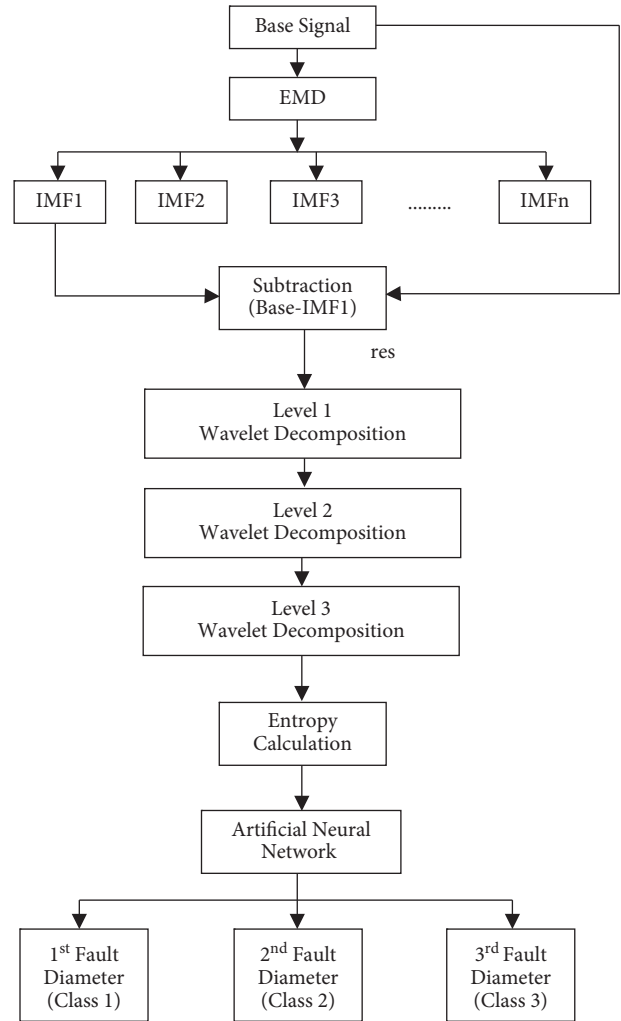


FIGURE 2: Structural outline of the proposed work.

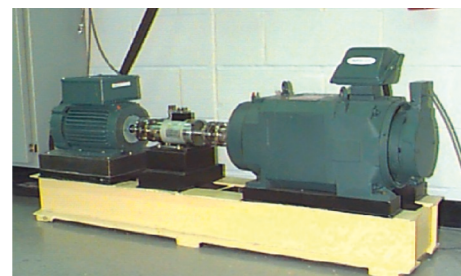


FIGURE 3: Test stand.

LPF and HPF to get second-order wavelet coefficients. In the proposed work, three-level wavelet decomposition has been done in order to get third-level wavelet coefficients [40].

The structural outline for the wavelet decomposition step is represented in Figure 1.

2.3. Features Based on Entropies. Entropy is used to measure uncertainty in the signal [41]. The unpredictability of time series is estimated by entropy.

The power spectrum of the signal was utilized by spectral entropy to determine the regularity of time series.

TABLE 1: Bearing specifications.

| Bearing | Inner diameter (inch) | Outer diameter (inch) | Ball diameter (inch) |
|-------------------|-----------------------|-----------------------|----------------------|
| Drive end bearing | 0.9843 | 2.0472 | 0.3126 |
| Fan end bearing | 0.6693 | 1.5748 | 0.2656 |

TABLE 2: Result of the proposed algorithm at different decomposition levels of DWTs.

| S.No. | Wavelet | Fault type | Fault diameter | Level 1 entropy | Level 2 entropy | Level 3 entropy |
|-------|------------|------------|----------------|-----------------|-----------------|-----------------|
| 1 | Daubechies | Inner race | 0.007 | 4.99402 | 4.96648 | 4.6139 |
| 2 | | Outer race | | 4.39204 | 3.84301 | 3.19669 |
| 3 | | Ball race | | 4.68635 | 5.15762 | 5.58455 |
| 4 | | Inner race | 0.014 | 5.44514 | 5.89579 | 6.25843 |
| 5 | | Outer race | | 4.61799 | 5.19792 | 5.78321 |
| 6 | | Ball race | | 4.51711 | 4.8739 | 5.13163 |
| 7 | | Inner race | 0.021 | 4.67998 | 4.08159 | 3.42083 |
| 8 | | Outer race | | 4.49768 | 4.19176 | 3.81456 |
| 9 | | Ball race | | 4.9763 | 5.53878 | 6.09507 |
| 1 | Haar | Inner race | 0.007 | 4.96365 | 4.98041 | 4.59873 |
| 2 | | Outer race | | 4.45668 | 3.94193 | 3.26267 |
| 3 | | Ball race | | 4.61941 | 5.09147 | 5.5482 |
| 4 | | Inner race | 0.014 | 5.45592 | 5.96977 | 6.26468 |
| 5 | | Outer race | | 4.56891 | 5.11679 | 5.71352 |
| 6 | | Ball race | | 4.47173 | 4.81214 | 4.98067 |
| 7 | | Inner race | 0.021 | 4.733 | 4.19014 | 3.54017 |
| 8 | | Outer race | | 4.48865 | 4.14026 | 3.68452 |
| 9 | | Ball race | | 4.88952 | 5.41589 | 5.92838 |
| 1 | Sym4 | Inner race | 0.007 | 4.9487 | 4.92179 | 4.49412 |
| 2 | | Outer race | | 4.3656 | 3.83343 | 3.14384 |
| 3 | | Ball race | | 4.61294 | 5.09549 | 5.49536 |
| 4 | | Inner race | 0.014 | 5.44833 | 5.95235 | 6.20637 |
| 5 | | Outer race | | 4.64124 | 5.21861 | 5.7934 |
| 6 | | Ball race | | 4.47653 | 4.79758 | 4.98408 |
| 7 | | Inner race | 0.021 | 4.68324 | 4.09673 | 3.44703 |
| 8 | | Outer race | | 4.49006 | 4.19583 | 3.70423 |
| 9 | | Ball race | | 4.94563 | 5.50294 | 6.02354 |
| 1 | Coif1 | Inner race | 0.007 | 4.96341 | 4.97298 | 4.66752 |
| 2 | | Outer race | | 4.39677 | 3.89673 | 3.30127 |
| 3 | | Ball race | | 4.65655 | 5.11717 | 5.53661 |
| 4 | | Inner race | 0.014 | 5.42136 | 5.948 | 6.2854 |
| 5 | | Outer race | | 4.62112 | 5.17604 | 5.83812 |
| 6 | | Ball race | | 4.44007 | 4.77809 | 5.02732 |
| 7 | | Inner race | 0.021 | 4.66871 | 4.1003 | 3.44436 |
| 8 | | Outer race | | 4.50012 | 4.25786 | 3.71598 |
| 9 | | Ball race | | 4.95024 | 5.51563 | 6.0299 |

Normalized Shannon entropy was used to evaluate the spectral entropy [24, 34]. Spectral entropy is the parameter to quantify spectral complexity of time series. Power spectral density (PSD) is defined as the power distribution of signal based on frequencies existing in signal. If the power level of each frequency component is represented by P_f , the ratio of the power level consistent to every frequency to total power $\sum P_f$ is called normalization of the power (np_f) and can be written as

$$np_f = \frac{P_f}{\sum P_f}. \quad (4)$$

Entropy is calculated by multiplication of power level according to every frequency and inverse logarithm of equal

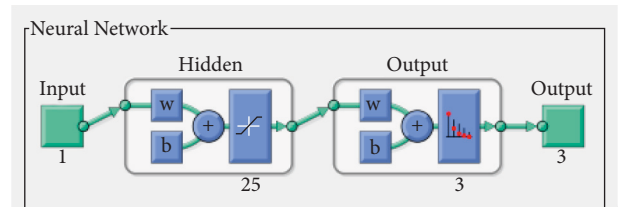


FIGURE 4: Neural network design used for the proposed method.

power level. Finally, spectral entropy ($ShEn1$) is calculated by [41]

$$ShEn1 = \sum P_f \log \frac{1}{P_f}. \quad (5)$$

TABLE 3: Result of the proposed algorithm at levels 1, 2, and 3 for various continuous wavelet types.

| S.No. | Wavelet | Fault diameter | Fault type | Level 1 entropy | Level 2 entropy | Level 3 entropy |
|-------|---------|----------------|------------|-----------------|-----------------|-----------------|
| 1 | meyr | 0.007 | Inner race | 4.62044 | 4.56986 | 3.93129 |
| 2 | | | Outer race | 4.64571 | 3.89411 | 3.38638 |
| 3 | | | Ball race | 4.03286 | 4.49054 | 4.54296 |
| 4 | | 0.014 | Inner race | 4.25968 | 4.61958 | 4.22894 |
| 5 | | | Outer race | 3.77234 | 4.29408 | 4.46133 |
| 6 | | | Ball race | 4.14535 | 4.5487 | 4.33351 |
| 7 | | 0.021 | Inner race | 4.77644 | 4.03004 | 3.08791 |
| 8 | | | Outer race | 4.74821 | 3.99134 | 3.87167 |
| 9 | | | Ball race | 4.02679 | 4.4618 | 4.243 |
| 1 | gaus1 | 0.007 | Inner race | 4.65305 | 4.67421 | 4.3627 |
| 2 | | | Outer race | 4.62621 | 4.6154 | 4.79962 |
| 3 | | | Ball race | 4.07647 | 4.07469 | 4.20235 |
| 4 | | 0.014 | Inner race | 4.29213 | 4.41689 | 4.30321 |
| 5 | | | Outer race | 3.86109 | 3.84888 | 4.4136 |
| 6 | | | Ball race | 4.14574 | 4.18351 | 4.34164 |
| 7 | | 0.021 | Inner race | 4.83451 | 4.77362 | 4.47731 |
| 8 | | | Outer race | 4.76385 | 4.56461 | 4.13111 |
| 9 | | | Ball race | 4.09455 | 4.13798 | 4.46649 |
| 1 | morl | 0.007 | Inner race | 4.61626 | 4.54568 | 3.84258 |
| 2 | | | Outer race | 4.58546 | 3.78241 | 3.33031 |
| 3 | | | Ball race | 4.02301 | 4.43336 | 4.25203 |
| 4 | | 0.014 | Inner race | 4.01912 | 4.4764 | 4.52151 |
| 5 | | | Outer race | 3.7788 | 4.25778 | 4.44057 |
| 6 | | | Ball race | 4.12073 | 4.56879 | 4.17328 |
| 7 | | 0.021 | Inner race | 4.78285 | 4.01478 | 3.20464 |
| 8 | | | Outer race | 4.73745 | 3.98008 | 3.30779 |
| 9 | | | Ball race | 4.00625 | 4.50274 | 4.29213 |
| 1 | mexh | 0.007 | Inner race | 4.65786 | 4.32452 | 4.22773 |
| 2 | | | Outer race | 4.63703 | 4.44181 | 4.23245 |
| 3 | | | Ball race | 4.09561 | 3.85489 | 3.7013 |
| 4 | | 0.014 | Inner race | 4.29233 | 4.13797 | 4.2346 |
| 5 | | | Outer race | 3.83845 | 3.65736 | 3.79228 |
| 6 | | | Ball race | 4.15931 | 4.02797 | 4.18802 |
| 7 | | 0.021 | Inner race | 4.81195 | 4.4722 | 4.11225 |
| 8 | | | Outer race | 4.78442 | 4.47225 | 4.1039 |
| 9 | | | Ball race | 4.08937 | 3.89522 | 4.12463 |

3. Proposed Method

This paper presents a novel scheme according to various entropy measures to classify the ball bearing fault. The data are randomly sampled to get different data size samples. The EMD has been applied to samples for the removal of high-frequency noisy component [42]. The high-frequency component has been deducted from raw signal to eliminate effectual noise. The complex vibration signal has been analysed in time-frequency domain for better accuracy of classification [43]. That raw signal is split into 2^3 subsignals, i.e., 8 scales with 3 levels of decomposition. The entropy of wavelet coefficients has been calculated which is utilized as feature for ball bearing fault's classification.

3.1. Proposed Algorithm. Let $r \rightarrow x(t)$, where $x(t)$ is sample comprising of population of vibrating data.

Sample space is arbitrarily picked from collection of population, and EMD is performed. EMD divides the

signal into IMFs, which are monotonic frequency components.

$$h(t) = \text{EMD}(r), \quad (6)$$

where $h(t)$ is a vector consisting of an IMF obtained using the EMD of signal space r .

The first IMF, i.e., the highest frequency component, is deducted from raw signal to obtain residue using the following equation:

$$\text{res} = r - h(t)\{1\}, \quad (7)$$

where res is the residue obtained after removing first IMF $[h(t)\{1\}]$, from signal space r .

Wavelet coefficients are obtained by transforming the residue (res) into the DWT up to third level of decomposition using equation (8). Equation (8) represents the mathematical model to calculate the DWT of the residue (res).

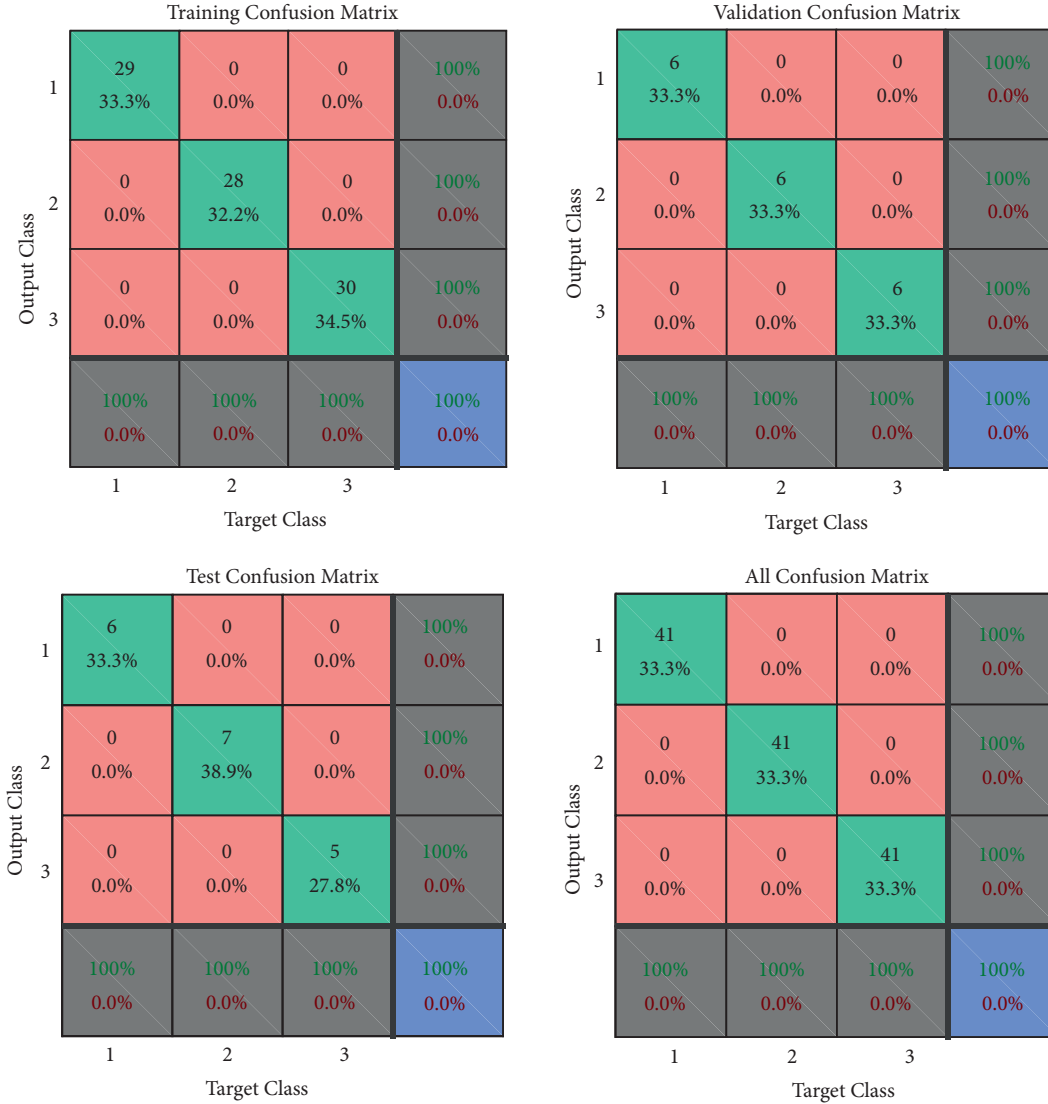


FIGURE 5: Confusion matrix for inner race fault set.

$$dwt_{res} = \frac{1}{\sqrt{2^j}} \int res \psi^* \left(\frac{t - k2^j}{2^j} \right) dt. \quad (8)$$

The entropy of the obtained wavelet coefficient (dwt_{res}) and maximum energy to Shannon entropy ratio are then evaluated as

$$E_n = - \sum_j P(dwt_{res}) \log P(dwt_{res}), \quad (9)$$

$$ShEn1 = P(dwt_{res}) \log \frac{1}{P(dwt_{res})}.$$

Calculated entropy for different set is utilized as an input parameter to neural network for classification.

The structural outline of the proposed technique is presented in Figure 2.

4. Results and Discussion

The data were obtained from Case Western Reserve University's Bearing Data Centre, United States. Arrangement of the machine is shown in Figure 3.

The specification and arrangement details are available in [35]. The test bearings used for the setup are of SKF and NTN make. The bearing information is provided in Table 1.

In the proposed algorithm, EMD is employed for removal of high-frequency noisy component. EMD decomposed a signal into IMF which varies from high frequency to low frequency. Initial IMF (IMF_1) is deducted from original signal (r) to get residue signal (res). Discrete wavelet transform of residue (res) is calculated up to 3rd level of decomposition. The entropy of the wavelet coefficient obtained after the 3rd level decomposition is calculated which is further utilized as a parameter to classify the ball bearing

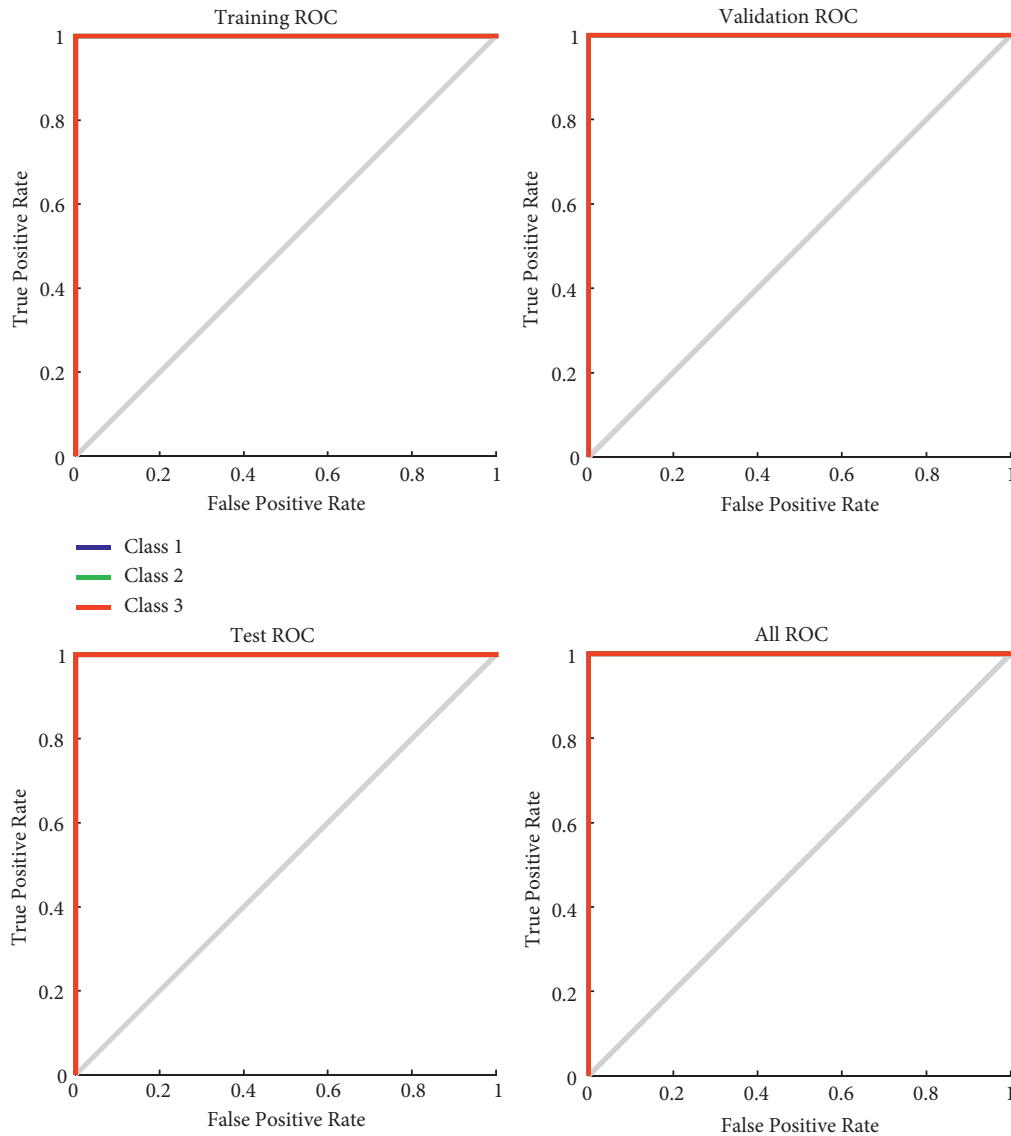


FIGURE 6: ROC for inner race fault set.

fault diameter into different output classes. The dataset has been split into subsets by choosing arbitrary samples. The proposed methodology has been tested for various CWT and DWT. The feature sets (entropy values) obtained from 3rd level wavelet coefficients are shown in Table 2 with respect to various discrete wavelets.

Feedforward neural network is utilized with 25 neurons in hidden layer. In the proposed work, feed-forward neural network has been used. Training of model has been done using the scaled conjugate gradient-based technique. Moller [36] developed the SCG algorithm, that is according to conjugate directions but does not do a line scan at every iteration like previous conjugate gradient algorithms [44]. Increasing computational cost of system [37]. SCG was created to eliminate the time-consuming process of searching for lines. The SCG method's step size is calculated by quadratic approximation of error function, making it extra robust and independent of user-

described parameter. The proposed algorithm has been tested over well-established dataset available online at [35]. The entire dataset has been separated into training and testing sets. For training, 70% of the dataset has been used and the remaining 30% is used for testing and validation. The accuracy of suggested algorithm is achieved after 10-fold cross validation. To validate the performance, cross entropy is used [45]. Three different sets for inner, outer, and ball race faults have been utilized as input parameters to neural network. The network has to classify input set into various fault diameter classes. The diameters of faults are 0.007 inch, 0.014 inch, and 0.021 inch. Figure 4 shows the neural network used to classify the input vector for the proposed method [46].

Tables 2 and 3 show the result of the proposed algorithm with discrete wavelets and continuous wavelets, respectively. The results obtained using CWT are depicted in Table 3. The outcomes of Tables 2 and 3 state that variation between the

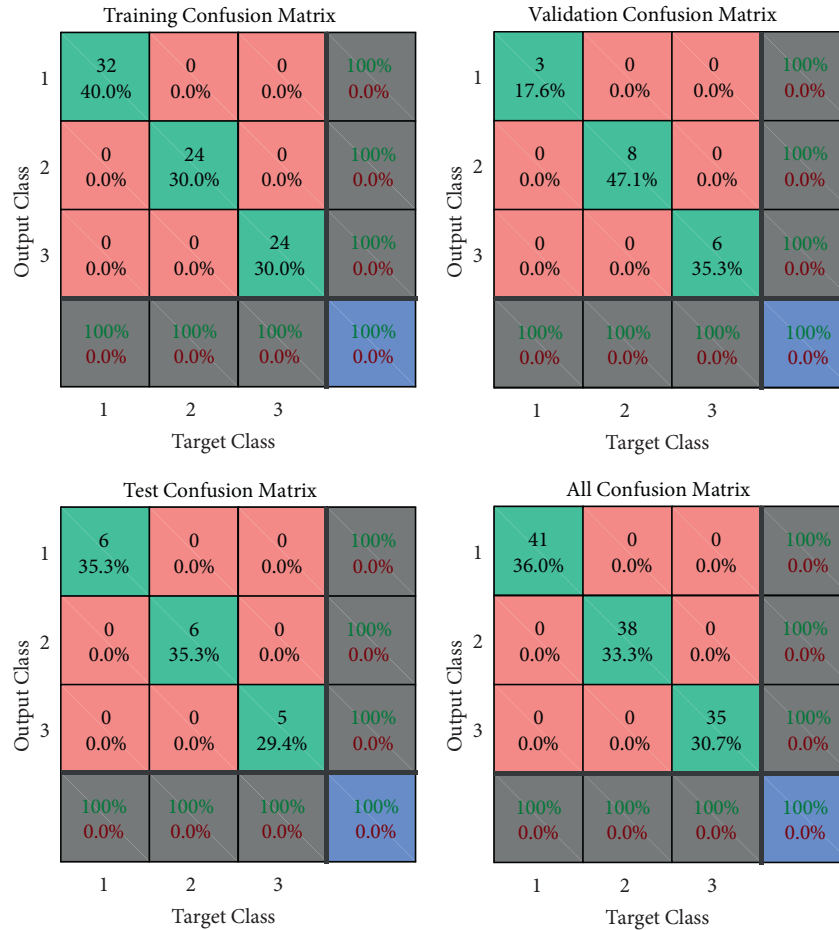


FIGURE 7: Confusion matrix for outer race fault set.

values of entropy with respect to fault diameter at various wavelets can be applied as a criterion for analysis of ball bearing fault diameter [47]. The confusion matrix and ROC for two sets are depicted in Figures 5–7. Figures 5 and 6 demonstrate confusion matrix and ROC for set obtained through entropy of inner race fault for the classification of fault diameter in bearings [48], and Figure 7 shows the confusion matrix for set obtained from entropy of outer race fault for classification [49] of fault diameter in the bearings. It can be concluded from Table 2 that for any kind of wavelet, when fault diameter changes from 0.007 to 0.014, in case of inner race, the entropy increases in the range of 30–40%, while for fault [50] diameter change from 0.014 to 0.021, the entropy [51] was found to be decreased in the range of 40–50%.

In case of outer race, when fault [52] diameter changes from 0.007 to 0.014, entropy increases by the value found in the range of 70–80%, while for 0.014 to 0.021 diameter change, entropy value decreases in the range of 30–40%. In case of ball race, when fault diameter changes from 0.007 to 0.014, entropy

decreases by the value found in the range of 5–10%, while for 0.014 to 0.021 diameter change, entropy value increases in the range of 15–20%.

5. Conclusion

This paper aims at determining the fault size and their correct classification. The authors present a new approach for diagnosis of bearing fault size by applying multiple decomposition techniques like EMD and wavelet decomposition. The EMD approach is utilized to divide original signal into monotonic frequency components. High-frequency components are deducted from the raw signal to get the residue whose wavelet decomposition is performed later. Therefore, EMD is utilized for the removal of high-frequency noisy component. The entropy associated with the third level wavelet coefficients of residue is calculated which is used to classify the ball bearing fault diameter into respective classes. Three fault diameters 0.007", 0.014", and 0.021" were considered. The results of the proposed technique as reflected in the confusion matrix prove

that the procedure used to classify the fault diameter size is more efficient than the empirical methods. With the proposed method, the achieved classification accuracy is about 100%. It can be concluded that when fault diameter increases from 0.007 to 0.014, inner race and outer race have increment in entropy value in particular range, while ball race has decrement in the value of entropy, whereas when fault diameter increases from 0.014 to 0.021, inner and outer race entropy has a decrement in specific range, while ball race entropy has been increased. Hence, on the basis of variation in entropy value for different kinds of fault, fault type as well as fault size can be diagnosed using the proposed algorithm.

Data Availability

The data that support the findings of this study are available on request from the corresponding author.

Conflicts of Interest

The authors declare that they have no conflicts of interest.

Acknowledgments

We would like to acknowledge Bearing Data Centre, University of Cleveland, Ohio, United States, for the raw data.

References

- [1] J. Chen, J. W. Wang, and X. K. Wu, "The application of some non-linear methods in rotating machinery fault diagnosis," *Mechanical Systems and Signal Processing*, vol. 15, pp. 697–705, 2001.
- [2] B. Samanta, K. R. Al-Balushi, and S. A. Al-Araimi, "Artificial neural networks and genetic algorithm for bearing fault detection," *Soft Computing*, vol. 10, no. 3, pp. 264–271, 2006.
- [3] S. A. Al-Araimi, K. R. Al-Balushi, and B. Samanta, "Bearing fault detection using artificial neural networks and genetic algorithm," *Journal of Applied Signal Processing*, vol. 3, pp. 366–377, 2004.
- [4] A. Ali Alnuaim, M. Zakariah, P. K. Shukla et al., "Human-computer interaction for recognizing speech emotions using multilayer perceptron classifier," *Journal of Healthcare Engineering*, vol. 2022, Article ID 6005446, 12 pages, 2022.
- [5] S. Janjarasjitt, H. Ocak, and K. A. Loparo, "Bearing condition diagnosis and prognosis using applied nonlinear dynamical analysis of machine vibration signal," *Journal of Sound and Vibration*, vol. 317, no. 1-2, pp. 112–126, 2008.
- [6] K. Feng, W. He, and Z. Jiang, "Rolling element bearing fault detection based on optimal antisymmetric real Laplace wavelet," *Measurement*, vol. 44, no. Issue 9, pp. 1582–1591, 2011.
- [7] B. Lazzarini, D. C. Stefanescu, and S. L. Volpi, "Time evolution analysis of bearing faults," in *Proceedings of the International Conference on Intelligent Systems and Control*, pp. 131–137, Cambridge MA, U.S, July 2009.
- [8] A. Ali Alnuaim, M. Zakariah, P. K. Shukla et al., "Human-computer interaction for recognizing speech emotions using multilayer perceptron classifier," *Journal of Healthcare Engineering*, vol. 2022, Article ID 6005446, 12 pages, 2022.
- [9] C. Bianchini, F. Immovilli, and M. Cocconcelli, "fault detection of linear bearings in brushless AC linear motors by vibration analysis," *IEEE Transactions on Industrial Electronics*, vol. 58, no. 5, pp. 1684–1694, 2011.
- [10] H. Lee and N. Nguyen, "Bearing fault diagnosis using adaptive network based fuzzy inference system," in *Proceedings of the International Symposium on Electrical & Electronics Engineering*, pp. 280–285, HCM City, Vietnam, October 2007.
- [11] A. Choudhury and N. Tandon, "A review of vibration and acoustic measurement methods for the detection of defects in rolling element bearings," *Tribology International*, vol. 32, no. 8, pp. 469–480, 1999.
- [12] C. Sridhar, P. Kumar Pareek, and R. Kalidoss, "Sajjad shaukat jamal, prashant kumar shukla, stephen jeswinde nuagah, "optimal medical image size reduction model creation using recurrent neural network and GenPSOWVQ," *Journal of Healthcare Engineering*, vol. 2022, Article ID 2354866, 8 pages, 2022.
- [13] R. Kumar Jha and P. D. Swami, "Intelligent fault diagnosis of rolling bearing and gear system under fluctuating load conditions using image processing technique," *Journal of Mechanical Science and Technology*, vol. 34, no. 10, pp. 4107–4115, 2020.
- [14] R. Kumar Jha, "Preety D Swami "Fault diagnosis and severity analysis of rolling bearings using vibration image texture enhancement and multiclass support vector machines"," *Applied Acoustics*, vol. 182, pp. 1–12, 2021.
- [15] A. Parey, M. El Badaoui, F. Guillet, and N. Tandon, "Dynamic modelling of spur gear pair and application of empirical mode decomposition-based statistical analysis for early detection of localized tooth defect," *Journal of Sound and Vibration*, vol. 294, no. 3, pp. 547–561, 2006.
- [16] A. Ali Alnuaim, M. Zakariah, C. Shashidhar et al., "Speaker gender recognition based on deep neural networks and ResNet50," *Wireless Communications and Mobile Computing*, vol. 2022, Article ID 4444388, 13 pages, 2022.
- [17] H. Li and Y. Yin, "bearing fault diagnosis based on Laplace wavelet transform," *TELKOMNIKA Indonesian Journal of Electrical Engineering*, vol. 10, no. 8, pp. 2139–2150, 2012.
- [18] J. Rafiee, M. A. Rafiee, and P. W. Tse, "Application of mother wavelet functions for automatic gear and bearing fault diagnosis," *Expert Systems with Applications*, vol. 37, no. 6, pp. 4568–4579, 2010.
- [19] P. K. Kankar, S. C. Sharma, and S. P. Harsha, "Rolling element bearing fault diagnosis using wavelet transform," *Neurocomputing*, vol. 74, no. 10, pp. 1638–1645, 2011.
- [20] P. K. Shukla and M. Dixit, "Cloud-based image fusion using guided filtering," in *Handbook of Research on Emerging Perspectives in Intelligent Pattern Recognition, Analysis, and Image Processing*, N. K. Kamila, Ed., pp. 146–165, IGI Global, Hershey, PA, 2016.
- [21] K. F. Al-Raheem, A. Roy, K. P. Ramachandran, D. K. Harrison, and S. Grainger, "Rolling element bearing faults diagnosis based on autocorrelation of optimized: wavelet de-noising technique," *International Journal of Advanced Manufacturing Technology*, vol. 40, no. 3-4, pp. 393–402, 2009.
- [22] H. Qiu, J. Lee, J. Lin, and G. Yu, "Wavelet filter-based weak signature detection method and its application on rolling element bearing prognostics," *Journal of Sound and Vibration*, vol. 289, no. 4, pp. 1066–1090, 2006.
- [23] W. He, Z. N. Jiang, and K. Feng, "Bearing fault detection based on optimal wavelet filter and sparse code shrinkage," *Measurement*, vol. 42, no. 7, pp. 1092–1102, 2009.

- [24] Z. K. Zhu, Z. He, A. Wang, and S. Wang, "Synchronous enhancement of periodic transients on polar diagram for machine fault diagnosis," *International Journal of Wavelets, Multiresolution and Information Processing*, vol. 7, no. 4, pp. 427–442, 2009.
- [25] P. Tiwari and P. Shukla, "A hybrid approach of TLBO and EBPNN for crop yield prediction using spatial feature vectors," *Journal of Artificial Intelligence*, vol. 1, no. 2, pp. 45–58, 2019.
- [26] W. T. Peter and D. Wang, "The automatic selection of an optimal wavelet filter and its enhancement by the new sparsogram for bearing fault detection: Part 2 of the two related manuscripts that have a joint title as "Two automatic vibration-based fault diagnostic methods using the novel sparsity measurement—parts 1 and 2"," *Mechanical Systems and Signal Processing*, vol. 40, no. 2, pp. 520–544, 2013.
- [27] K. F. Al-Raheem, A. Roy, K. P. Ramachandran, D. K. Harrison, and S. Grainger, "Application of the Laplace-wavelet combined with ANN for rolling bearing fault diagnosis," *Journal of Vibration and Acoustics*, vol. 130, no. 5, Article ID 51007, 2008.
- [28] H. Hong and M. Liang, "Fault severity assessment for rolling element bearings using the Lempel–Ziv complexity and continuous wavelet transform," *Journal of Sound and Vibration*, vol. 320, no. 1, pp. 452–468, 2009.
- [29] S. Stalin, P. Maheshwary, and P. kumar Shukla, "An Improved NVSS Scheme Based on Blocked Compression Scheme," *Journal of Advanced Research in Dynamical and Control Systems*, no. 13, pp. 960–966, 2008.
- [30] P. Konar and P. Chattopadhyay, "Bearing fault detection of induction motor using wavelet and Support Vector Machines (SVMs)," *Applied Soft Computing*, vol. 11, no. 6, pp. 4203–4211, 2011.
- [31] P. K. Kankar, S. C. Sharma, and S. P. Harsha, "Rolling element bearing fault diagnosis using autocorrelation and continuous wavelet transform," *Journal of Vibration and Control*, vol. 17, no. 14, pp. 2081–2094, 2011.
- [32] C. Li, M. Liang, Y. Zhang, and S. Hou, "Multi-scale autocorrelation via morphological wavelet slices for rolling element bearing fault diagnosis," *Mechanical Systems and Signal Processing*, vol. 31, pp. 428–446, 2012.
- [33] R. Singh, P. Shukla, and P. Rawat, "Prashant kumar shukla, "invisible medical image watermarking using edge detection and discrete wavelet transform coefficients"," *International Journal of Innovative Technology and Exploring Engineering (IJITEE)*, vol. 9, no. 1, pp. 5074–5580, 2019.
- [34] P. Kumar Pareek, C. Sridhar, and R. Kalidoss, "Muhammad aslam, manish maheshwari, prashant kumar shukla, stephen jeswinde nuagah, "IntOPMICM: intelligent medical image size reduction model"," *Journal of Healthcare Engineering*, vol. 2022, Article ID 5171016, 11 pages, 2022.
- [35] R. Yan and R. Gao, "Performance evaluation of complex-valued wavelet basis on vibration analysis for bearing defect diagnosis," *International Journal of Comprehensive Engineering, Part A: Maintenance Engineering*, vol. 1, pp. 41–47, 2012.
- [36] H. Liu, X. Wang, and C. Lu, "Rolling bearing fault diagnosis under variable conditions using Hilbert-Huang transform and singular value decomposition," *Mathematical Problems in Engineering*, vol. 2014, Article ID 765621, 10 pages, 2014.
- [37] L. Y. Lei and Q. Zhang, "Relevance vector machine based bearing fault diagnosis," in *Proceedings of the of IEEE International Conference on Machine Learning and Cybernetics*, pp. 3492–3496, Dalian, China, August 2006.
- [38] N. E. Huang, Z. Shen, S. R. Long et al., "The empirical mode decomposition and the Hilbert spectrum for nonlinear and non-stationary time series analysis," *Proceedings of the Royal Society of London: Mathematical, Physical and Engineering Sciences*, vol. 454, no. 1971, pp. 903–995, 1998.
- [39] R. Singh, P. Rawat, and P. Shukla, "Robust medical image authentication using 2-D stationary wavelet transform and edge detection," in *Proceedings of the 2nd IET International Conference on Biomedical Image and Signal Processing (ICBISP 2017)*, pp. 1–8, Wuhan, China, May 2017.
- [40] G. B. Huang, Q. Y. Zhu, and C. K. Siew, "Extreme learning machine: a new learning scheme of feedforward neural networks," in *Proceedings of the IEEE International Joint Conference on Neural Networks*, pp. 985–990, Budapest, Hungary, July 2004.
- [41] R. Dubey and D. Agrawal, "Bearing fault classification using ANN-based Hilbert footprint analysis," *IET Science, Measurement & Technology*, vol. 9, no. 8, pp. 1016–1022, 2015.
- [42] J. Seshadrinath, B. Singh, and B. K. Panigrahi, "Investigation of vibration signatures for multiple fault diagnosis in variable frequency drives using complex wavelets," *IEEE Transactions on Power Electronics*, vol. 29, no. 2, pp. 936–945, 2014.
- [43] N. Kannathal, M. L. Choo, U. R. Acharya, and P. K. Sadasivan, "Entropies for detection of epilepsy in EEG," *Computer Methods and Programs in Biomedicine*, vol. 80, no. 3, pp. 187–194, 2005.
- [44] C. E. Shannon, "A mathematical theory of communication," *ACM SIGMOBILE - Mobile Computing and Communications Review*, vol. 5, no. 1, pp. 3–55, 2001.
- [45] J. Fell, J. Röschke, K. Mann, and C. Schäffner, "Discrimination of sleep stages: a comparison between spectral and nonlinear EEG measures," *Electroencephalography and Clinical Neurophysiology*, vol. 98, no. 5, pp. 401–410, 1996.
- [46] Møller and M. Fodslette, "A scaled conjugate gradient algorithm for fast supervised learning," *Neural Networks*, vol. 6, no. 4, pp. 525–533, 1993.
- [47] A. Ali Alnuaim, M. Zakariah, A. Alhadlaq et al., "Human-computer interaction with detection of speaker emotions using convolution neural networks," *Computational Intelligence and Neuroscience*, vol. 2022, Article ID 7463091, 16 pages, 2022.
- [48] L. Babani, S. Jadhav, and B. Chaudhari, "Scaled conjugate gradient based adaptive ANN control for SVM-DTC induction motor drive," in *Proceedings of the IFIP International Conference on Artificial Intelligence Applications and Innovations*, pp. 384–395, Springer, Hersonissos, Crete, Greece, June 2016.
- [49] X. Yuan and T. Zhang, "fault diagnosis for rotating machinery based on convolutional neural network and empirical mode decomposition," *Shock and Vibration*, vol. 2017, Article ID 3084197, 12 pages, 2017.
- [50] D. Belmiloud, T. Benkedjouh, M. Lachi, A. Laggoun, and J. P. Dron, "Deep convolutional neural networks for Bearings failure prediction and temperature correlation," *Journal of Vibroengineering*, vol. 20, no. 8, pp. 2878–2891, 2018.
- [51] R. Magar, L. Ghule, J. Li, Y. Zhao, and A. B. Farimani, "FaultNet: a deep convolutional neural network for bearing fault classification," *IEEE Access*, vol. 9, Article ID 25189, 2021.
- [52] S. Zhang, S. Zhang, B. Wang, and T. G. Habetler, "Deep learning algorithms for bearing fault diagnostics—a comprehensive review," *IEEE Access*, vol. 8, Article ID 29857, 2020.